Phase Transformation Guided Single-Layer β-$Co(OH)_2$ Nanosheets for Pseudocapacitive Electrodes

Lei Wang,[†,‡] Chong Lin,[†] Fengxing Zhang,[‡] and Jian Jin[†,*]

[†]i-LAB and Nano-Bionics Division, Suzhou Institute of Nano-Tech and Nano-Bionics, Chinese Academy of Sciences, Suzhou, Jiangsu, 215123, China and [‡]Key Laboratory of Synthesis and Natural Functional Molecular Chemistry (Minnistry of Education), College of Chemistry & Materials Science, Northwest University, Xi'an, Shaanxi 710069, China

ABSTRACT It is known that $Co(OH)_2$ can be crystallized into a layered structure with two polymorphs: α and β. The single-layer α-$Co(OH)_2$ nanosheet has been prepared by exfoliating directly α phase layered $Co(OH)_2$. However, due to theoretical barriers, a single-layer β-$Co(OH)_2$ nanosheet has not been achieved so far. In this article, phase transformation during exfoliation of layered $Co(OH)_2$ from α to β is observed and a single-layer β-$Co(OH)_2$ nanosheet with a thickness of ~1.1 nm is prepared through phase transition of layered α-$Co(OH)_2$ nanocones in a mild wet chemical process for the first time, with a nearly 100% yield. The as-prepared single-layer β-$Co(OH)_2$ nanosheets are assembled with graphene oxide to form an all-two-dimensional materials-based composite for use as an electrode for the pseudocapacitor. The reduced graphene oxide/β-$Co(OH)_2$ composite exhibits a high specific capacitance up to 2080 F/g scaled to the total mass of the electrode or 3355 F/g scaled to the active mass of β-$Co(OH)_2$ nanosheets at the current density of 1 A/g. The electrode also demonstrates the excellent rate performance and long cycle life.

KEYWORDS: single-layer β-$Co(OH)_2$ nanosheet · two-dimensional materials · pseudocapacitors

Recent research has shown that, in addition to the composition and arrangement of atoms in materials, dimensionality plays a crucial role in determining their fundamental properties. This has been most strikingly highlighted by two-dimensional (2D) graphene over the past few years, which exhibits exotic condensed-matter phenomena that are absent in bulk graphite.[1−5] The rapid pace of progress in graphene and the methodology developed[6−9] in preparing ultrathin layers of other types of materials with/without lamellar structures similar to that of graphite, such as transition metal dichalcogenides,[10−15] germanium,[16,17] layered transition metal (hydro) oxides,[18−25] and so on,[26−37] have received significant attention.

$Co(OH)_2$, a member of layered transition metal hydroxides, can be crystallized into a layered structure with two polymorphs: α and β.[38] In α phase, a pair of Co tetrahedral sites is occupied by the anion and is generated both above and below one octahedral vacancy, sharing three hydroxyl ions with other neighboring octahedrals. It consists of a positively charged layer with anions and water molecules residing in the gallery to restore charge neutrality. The β phase possesses a brucite-like origin, where octahedral with divalent cobalt cations six-fold coordinated by hydroxyl ions share edges to produce 2D charge-neutral layers stacked one over the other without any anion. In principle, layered α-$Co(OH)_2$ could be exfoliated into single-layer α-$Co(OH)_2$ nanosheets (NSs) directly. Very recently, the pure phase of single-layer α-$Co(OH)_2$ NSs was obtained through exfoliation of layered α-$Co(OH)_2$ nanocones by Ma and co-workers, who demonstrated their unique optical property.[39] Unfortunately, due to the theoretical barrier, where layered β-$Co(OH)_2$ has a close structure and the host layers are held together by robust van der Waal's force, layered β-$Co(OH)_2$ is considered difficult to exfoliate into single-layer β-$Co(OH)_2$ NSs.[40,41] To date, there is no report about preparation of single-layer β-$Co(OH)_2$ NSs. Due to different crystal structure from single-layer α-$Co(OH)_2$ NSs, there is a reason to believe that single-layer β-$Co(OH)_2$ NSs probably own astonishing properties.

* Address correspondence to jjin2009@sinano.ac.cn.

Received for review January 21, 2014 and accepted March 6, 2014.

Published online March 06, 2014
10.1021/nn500386u

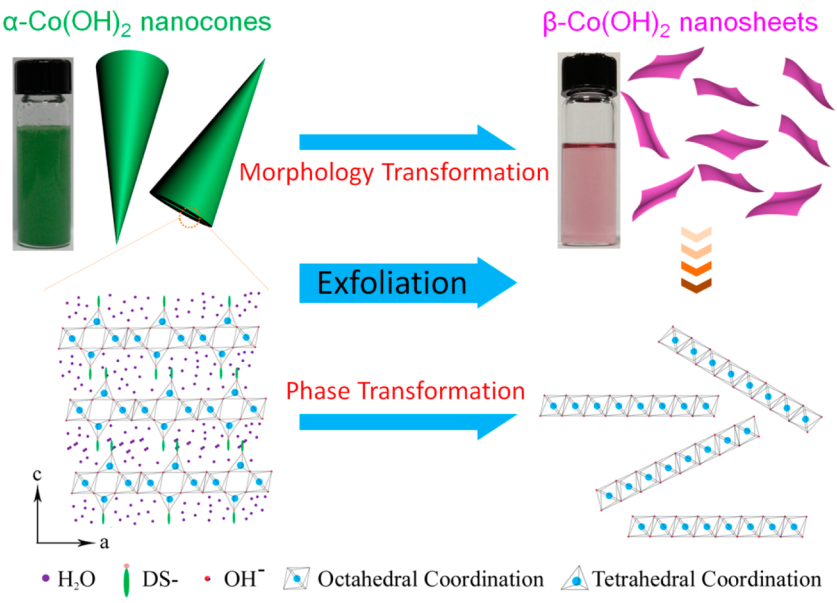

Scheme 1. Preparation of single-layer β-Co(OH)$_2$ NSs. Optical photograph and the structure models along the *b axis of layered α-Co(OH)$_2$ nanocones and single-layer β-Co(OH)$_2$ NSs, respectively.**

As a member of transition metal hydroxide, Co(OH)$_2$ is a promising pseudocapacitive material, which could deliver a very high theoretical capacitance during two steps of reversible redox reactions of cobalt ion (CoII ↔ CoIII ↔ CoIV). Recent advances in nanotechnologies have greatly achieved the development of Co(OH)$_2$-based high-performance pseudocapacitor electrodes.[42−50] Despite significant progress, however, techniques to realize the full potential of electrode materials by achieving simultaneously tailored electrode structure and conductivity are still required and have become a goal. As pseudocapacitance arises from reversible redox reactions, it is highly desirable to reduce the size and increase the surface area of Co(OH)$_2$ so that the diffusion length for electrons and ions in a single particle is shortened and a high flux of electrons and ions is allowed. Therefore, it is expected that single-layer Co(OH)$_2$ NSs would exhibit a superior capacitance when used as pseudocapacitive materials than the bulk Co(OH)$_2$.[51] Although α-Co(OH)$_2$ phase could be exfoliated into single-layer, the coordinated anions on Co tetrahedral sites would decrease specific capacitance due to their lack of electrochemical activity. Instead, the non-anion-coordinated single-layer β-Co(OH)$_2$ NSs with rational designed structure should be able to display an excellent electrochemical performance.

In this work, we report for the first time the synthesis of single-layer β-Co(OH)$_2$ NSs with the thickness of ~1.1 nm by a wet chemistry process and investigation of the performance of β-Co(OH)$_2$ NSs as a pseudocapacitive material. Considering that Co(OH)$_2$ is an insulator, hybridizing Co(OH)$_2$ with conductive materials could be an effective way to improve conductivity so as to obtain higher specific capacitance. Owing to the intrinsic properties of lightweight, good conductivity, and large surface area of reduced graphene oxide (RGO),[52−54] the β-Co(OH)$_2$ NSs are thus assembled with RGO to form an all-2D materials-based composite for the use of electrode material for pseudocapacitors. Recent results also showed that the RGO could be stabilized both the electrochemical and mechanical properties of Co(OH)$_2$.[48,49] As a consequence, the electrode exhibits an unprecedentedly high specific capacitance of 2080 F/g scaled to the total mass of the electrode or 3355 F/g scaled to the active mass of Co(OH)$_2$ at current density of 1 A/g.

RESULTS

Scheme 1 demonstrates the optical images and the structural model of as-prepared layered α-Co(OH)$_2$ nanocones and β-Co(OH)$_2$ NSs. As is shown, the α phase consists of positive charge layers with various anions (the anion is dodecyl sulfate in this work) and water molecules residing in the gallery to restore charge neutrality. This causes a substantial expansion in the interlayer spacing (>8 Å), and the color is green. On the contrast, the β phase possesses a brucite-like origin, and the color is pink. The synthesis route from layered α-Co(OH)$_2$ nanocones into single-layer β-Co(OH)$_2$ NSs is as follows: (i) layered α-Co(OH)$_2$ nanocones were first synthesized, and (ii) then they are exfoliated in formamide at 80 °C under nitrogen gas protection. In the exfoliation process, a color change of solution from green, which corresponds to layered α-Co(OH)$_2$ nanocones, to pink, which corresponds to single-layer β-Co(OH)$_2$ NSs, could be observed, indicating the occurrence of phase transformation of Co(OH)$_2$.

Figure 1 depicts the structure and morphology characterization of as-prepared layered α-Co(OH)$_2$. A large

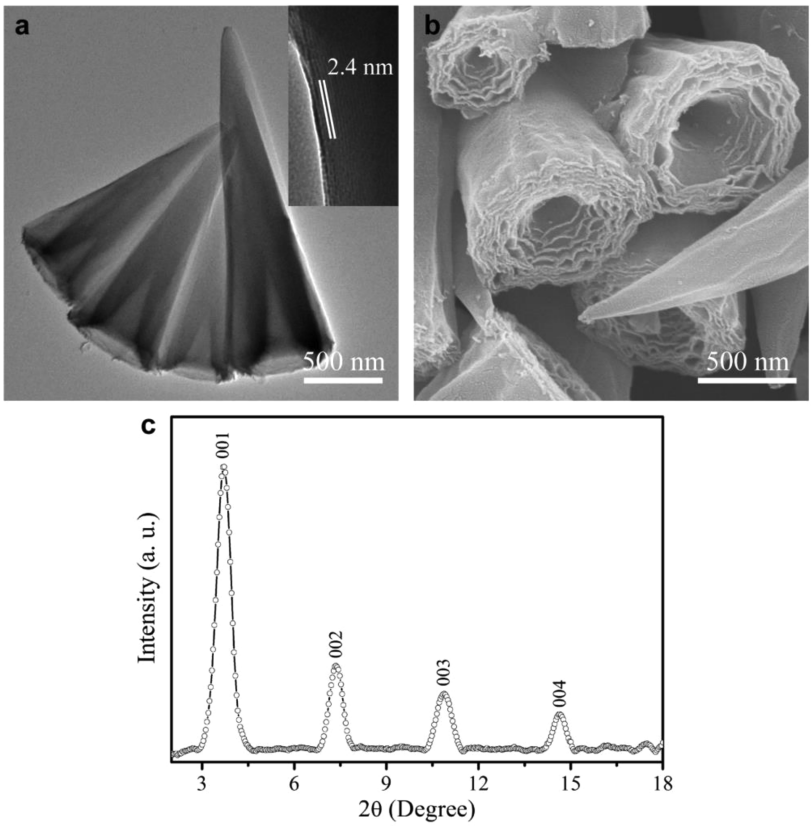

Figure 1. Structural characterization of as-prepared layered α-$Co(OH)_2$ nanocones. (a) TEM, (inset) HRTEM, (b) SEM image, and (c) XRD pattern.

amount of nanocones with uniform structure and smooth surface are observed in transmission electron microscopy (TEM) images (Figure 1a). The nanocones have an average bottom diameter of approximately 0.5 μm and a length of around 3 μm. Inset of Figure 1a is a high-resolution TEM (HRTEM) image which shows an ordered multilayered structure with adjacent-layer spacing of 2.4 nm. Figure 1b clearly demonstrates that the nanocones possess multilayered structure with hollow interior. The formation of layered α-$Co(OH)_2$ nanocones is assumed to undergo a similar process as described in previous work.[39] Dodecyl sulfate intercalated lamellar structures with few layers are first formed and then curl up at the edge, which produce a conical angle rather than a tubular structure owing to their morphological feature and lower energy barrier. The ordered multilayer structure of α-$Co(OH)_2$ nanocones is also confirmed by X-ray diffraction (XRD) (Figure 1c). Previous results have confirmed that the thickness of a single layer of layered hydroxide NSs is ~0.8 nm.[51] Therefore, the distance between adjacent layers of layered α-$Co(OH)_2$ nanocones is calculated to be 1.6 nm. When the molecular length of dodecyl sulfate (calculated to ~1.9 nm) is taken into consideration, it is inferred that the dodecyl sulfate ions arrange perpendicularly to cobalt hydroxide nanosheets with a tilt angle of ~25°.[50]

The synthesis of layered α-$Co(OH)_2$ nanocones and exfoliation of them into single-layer α-$Co(OH)_2$ NSs has recently been reported by Ma *et al.*[39] Different from his process, we achieved in this work the exfoliation of layered α-$Co(OH)_2$ nanocones into single-layer β-$Co(OH)_2$ NSs by slightly changing the experimental condition where layered α-$Co(OH)_2$ nanocones were first synthesized by refluxing hexamethylenetetramine (HMT) for 5 h, and exfoliation was then conducted in formamide at 80 °C under nitrogen gas with continuous stirring. During the exfoliation process, a color change from green solution, which corresponds to α-$Co(OH)_2$, to pink solution, which corresponds to β-$Co(OH)_2$, within 15 h could be observed (Figure 2a), indicating the occurrence of phase transformation of $Co(OH)_2$ from α to β. Corresponding UV−vis absorption of the solutions with reaction time shows that the peak for tetrahedral coordination of Co around 630 nm disappears after 15 h (Figure 2b). To further prove the formation of β-$Co(OH)_2$ NSs, α-$Co(OH)_2$ NSs were also prepared according to a previously reported method. The UV−vis absorption spectra of α-$Co(OH)_2$ NSs and β-$Co(OH)_2$ NSs are shown together in Figure 2c for comparison. It can be seen that, for α-$Co(OH)_2$ NSs, two peaks around 520 and 630 nm are observed due to the octahedral and tetrahedral coordination of Co. For β-$Co(OH)_2$ NSs, only one peak around 520 nm is obtained and no absorption around 630 nm ascribed to tetrahedral coordination of Co^{2+} in α phase is observed.[39] This means that α phase $Co(OH)_2$ has

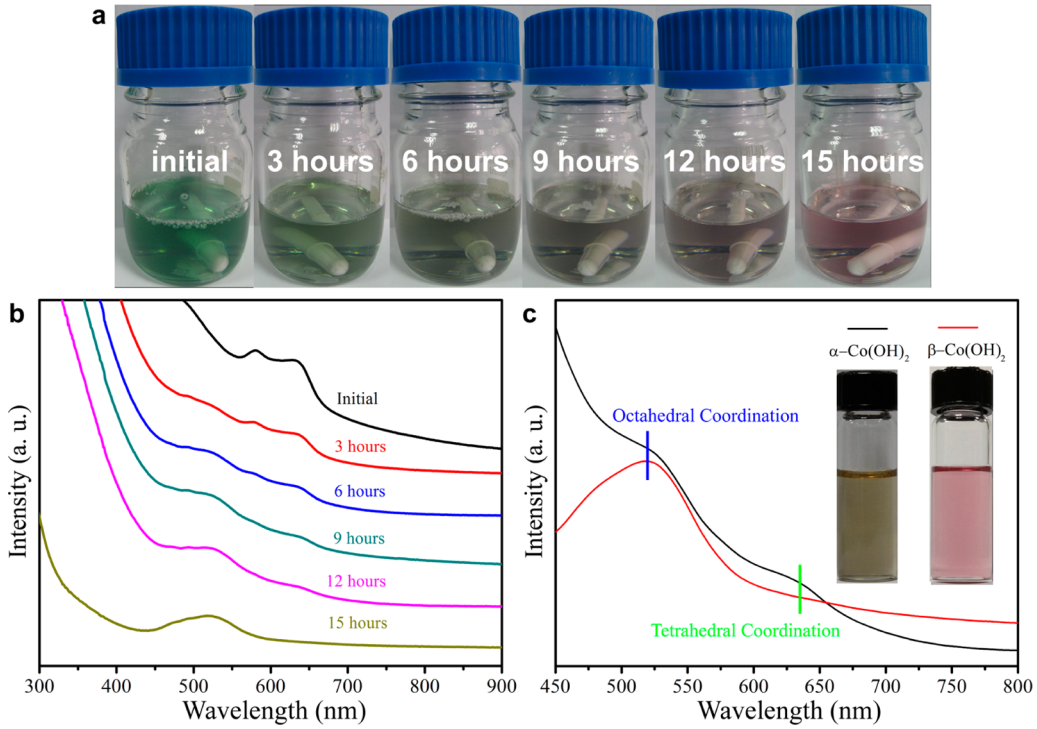

Figure 2. Optical characterization of the exfoliation of layered α-$Co(OH)_2$ nanocones. (a) Color evolution during exfoliating process of layered α-$Co(OH)_2$ nanocones. (b) Variation of UV−vis absorption spectra of layered α-$Co(OH)_2$ nanocone dispersion with exfoliation time. (c) UV−vis absorption spectra of single-layer α-$Co(OH)_2$ NSs (black line) and single-layer β-$Co(OH)_2$ NSs (red line). The insets are the digital photographs of the two dispersions correspondingly.

converted to β phase $Co(OH)_2$ completely. It is noteworthy that the pink color corresponding to β-$Co(OH)_2$ NS solution is highly stable even for a half of a year. In contrast, exfoliation of α-$Co(OH)_2$ nanocones in formamide at room temperature instead of 80 °C was also carried out. It was found that the color change from green to pink could also occur but took a much longer time of up to 7 days under this condition. It reveals that the higher exfoliation temperature is advantageous to shorten the exfoliation time. From another point of view, this result also shows that the phase transformation from α to β follows the Ostwald's rule of stages, which says that crystal always transforms from thermodynamically unstable phases to thermodynamically stable phase.[55] The α phase of $Co(OH)_2$ is a metastable crystalline feature as compared to β phase.[40] The phase transformation from α to β during exfoliation is a process from thermodynamically unstable to thermodynamically stable.

To further investigate the phase transformation from α to β phase, layered α-$Co(OH)_2$ was also prepared by a hydrothermal method (see Supporting Information for detailed description). The morphology of the as-prepared layered α-$Co(OH)_2$ with conic shape is similar to those prepared by our reflux method and reported by others[39] (Figure S2). It is acknowledged that reflux process usually produces a material with lower crystallinity than microwave and hydrothermal method. Therefore, single-layer α-$Co(OH)_2$ NSs could be obtained by exfoliating the layered α-$Co(OH)_2$ nanocones prepared by the hydrothermal method due to the improvement of the stability of crystalline structure. However, we found that such single-layer α-$Co(OH)_2$ NSs are not stable enough for a long time even at room temperature. The color of the dispersion of single-layer α-$Co(OH)_2$ NSs changes gradually from yellow-green (caused by octahedral and tetrahedral coordination of Co^{2+}) to pink (caused by tetrahedral coordination of Co^{2+}) after ~30 days, indicating the phase transformation from α to β. At a high temperature (such as 80 °C), the phase transformation becomes much faster. The phase transformation from α to β could be complete within ~3 days. We thus conclude that, whether the layered α-$Co(OH)_2$ nanocones are prepared by the hydrothermal method or reflux method, single-layer β-$Co(OH)_2$ NSs are the final product after exfoliation and remain stable for long-term. Meanwhile, the morphology transformation was also characterized during exfoliation (Figure 3). The expansion of a $Co(OH)_2$ nanocone after 3 h exfoliation can be clearly seen. Many wrinkles could be observed on the surface of the nanocone (Figure 3b). After exfoliation for 6 h, the conic structure is hard to distinguish and a sheet-like structure appears (Figure 3c). After exfoliation for 9 h, there is no sign of conic structure and morphology transformation is completed. Combining with the data of UV−vis spectra, as shown in Figure 2, we conclude that the phase transformations from α to β and the morphology transformations from cone to sheet are carried out simultaneously.

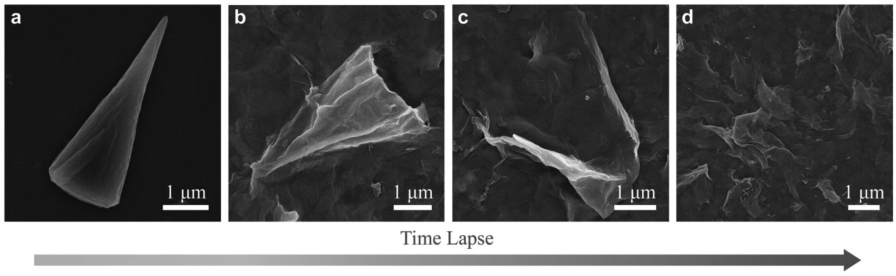

Figure 3. SEM images of layered α-Co(OH)$_2$ nanocones during exfoliation at initial (a) and after 3 h (b), 6 h (c), and 9 h (d).

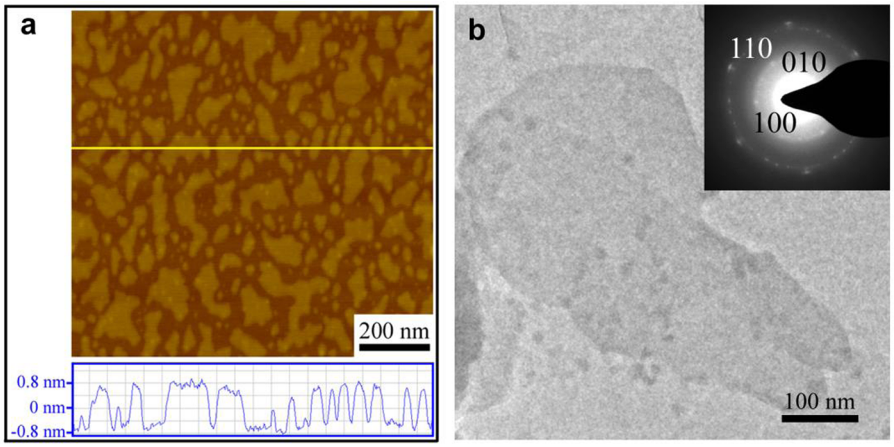

Figure 4. Structural characterization of single-layer β-Co(OH)$_2$ NSs. (a) AFM and height profile, (b) TEM and SAED images (inset of b).

The obtained β-Co(OH)$_2$ NSs were further examined by TEM and atomic force microscopy (AFM). The sheet-like structures with lateral size from several tens to several hundred nanometers and thickness in the range of 0.9−1.3 (1.1 ± 0.2 in average) nm are clearly seen in a wide visual range (Figure 4). The selected area electron diffraction (SAED) image taken from an individual nanosheet corresponds to the crystalline structure of β-Co(OH)$_2$ (inset of Figure 4b). These results prove the formation of crystalline single-layer β-Co(OH)$_2$ NSs.

GO/β-Co(OH)$_2$ NS composite was prepared by directly mixing β-Co(OH)$_2$ NSs dispersed in formamide and GO dispersed in water. Clear Tyndall light scattering is discerned for the two dispersions, indicating the presence of well-dispersed colloidal sheets in formamide and water (Figure 5a,b). As β-Co(OH)$_2$ NSs are positively charged and GO could be considered to be negatively charged due to the presence of carboxylate, the GO/β-Co(OH)$_2$ NS composite could be produced spontaneously under the electrostatic attraction force by mixing the two dispersions as shown in Figure 5c. The zeta-potentials of the two dispersions are 47 mV for β-Co(OH)$_2$ NSs and −49 mV for GO (Figure S3), indicating they have matched surface charges. In principle, the electrostatic interaction between GO and single-layer β-Co(OH)$_2$ NSs could create a layered assembly of two types of sheets. The obtained GO/β-Co(OH)$_2$ NS composite was finally reduced to the RGO/β-Co(OH)$_2$ NS composite at 180 °C under Ar$_2$/H$_2$ mixing gas (5 wt % H$_2$) for use as a pseudocapacitive electrode.

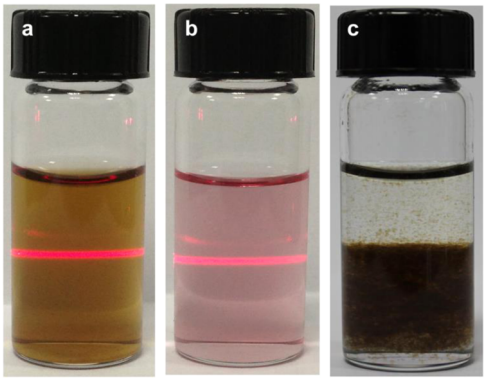

Figure 5. Digital photographs of the dispersions of GO (a), single-layer β-Co(OH)$_2$ NSs (b), and mixture of GO/β-Co(OH)$_2$ NSs (c).

The morphology and composition of RGO/β-Co(OH)$_2$ NS composites were characterized as shown in Figure 6. The SEM and TEM images show clearly the multilayer structure composed of sheet-like components, especially at the edge site of the composite (Figure 6a,b). SAED taken on the composite shows a diffraction circle and several diffraction dots which correspond to β-Co(OH)$_2$ and RGO, respectively (inset of Figure 6b). Dark-field scanning transmission electron microscopy (DF-STEM) image and corresponding elemental mapping images demonstrate that the elements C, O,

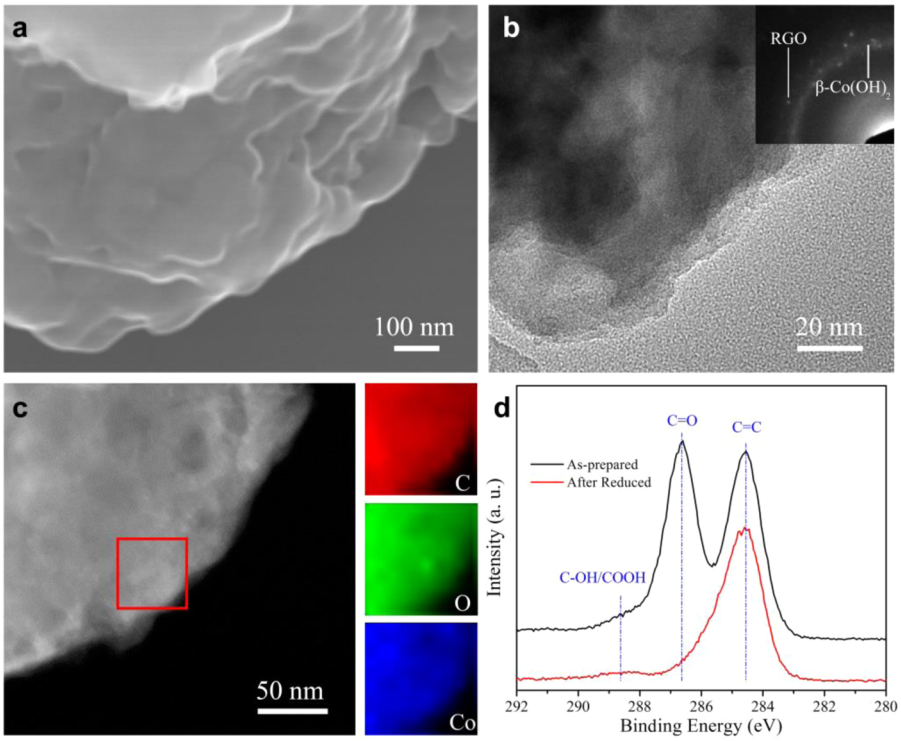

Figure 6. Morphology characterization of RGO/β-Co(OH)$_2$ NS composite. (a) SEM, (b) TEM and SAED (inset of b), (c) DF-STEM and corresponding elemental mapping images, and (d) C 1s XPS spectra of GO/β-Co(OH)$_2$ NS composite and RGO/β-Co(OH)$_2$ NS composite.

and Co are evenly distributed in the whole sample (Figure 6c). X-ray photoelectron spectroscopy (XPS) was used to investigate the degree of reduction of GO in the composite, as shown in Figure 6d. The as-prepared GO/β-Co(OH)$_2$ NS composite gives three C 1s peaks located at 284.6 eV to C═C of sp^2-hybridized carbon atoms, 286.8 eV to C−OH and/or C═O bond, and 288.8 eV to COOH bond. After reduction, there are almost no oxygenated species of C 1s peaks, revealing the reduction of GO to RGO. Thermogravimetric analysis (TGA) was used to determine the mass ratio of RGO and β-Co(OH)$_2$ in the composite. It is calculated that the mass ratio of RGO and β-Co(OH)$_2$ in the composite is 38:62 (see Figure S4 and detailed description therein).

Electrochemical measurements were made on a three-electrode cell setup that consists of a working electrode, a platinum wire counter electrode, a calomel reference electrode and 2 M KOH aqueous solution as electrolyte. First, the electrochemical properties of layered α-Co(OH)$_2$ nanocones, single-layer β-Co(OH)$_2$ NSs, and RGO/β-Co(OH)$_2$ NSs composite-based electrodes were measured (Figure 7). It is worthy to note that the preparation of RGO/α-Co(OH)$_2$ NS composite did not succeed due to unmatched surface charges between GO dispersion (zeta-potential = −49 mV) and single-layer α-Co(OH)$_2$ NS dispersion (zeta-potential = 32 mV) (Figure S3). Figure 7a shows their cyclic voltammetry (CV) curves. Apparently, all three electrodes show two current peaks which correspond to redox faradic reaction, indicating the pseudocapacitive characteristic of metal hydroxide-based electrode materials. This is distinct from that of the electric double-layer capacitance which usually produces a CV curve close to a smooth rectangular shape. The appearance of two redox peaks also reveals that pseudocapacitive Co(OH)$_2$ contributes mainly to the capacitance of the composite electrode. The observation of two redox peaks means that there are two quasi-reversible electron-transfer processes in the electrode. The potential differences in the two pairs of anodic peaks and cathodic peaks are both larger than 0.1 V. Theoretically, for a reversible single-electron-transfer redox process in solution, the potential difference in a pair of anodic peaks and cathodic peaks is expected to be 0.058 V. Therefore, there are two plausible reactions for all three types of electrodes as shown below:

$$Co(OH)_2 + OH^- = CoOOH + H_2O + e \quad (1)$$

$$CoOOH + OH^- = CoO_2 + H_2O + e \quad (2)$$

Our previous work shows that the electrochemical performance of layered Co(OH)$_2$ is inseparable from their morphology.[50] In this work, the interlayer distance of layered α-Co(OH)$_2$ nanocones is ~1.6 nm, which could serves as "ion-buffering reservoirs" of electrolyte ions during the electrochemical process. Two electrons could be transferred during the electrochemical process, resulting in higher pseudocapacitance

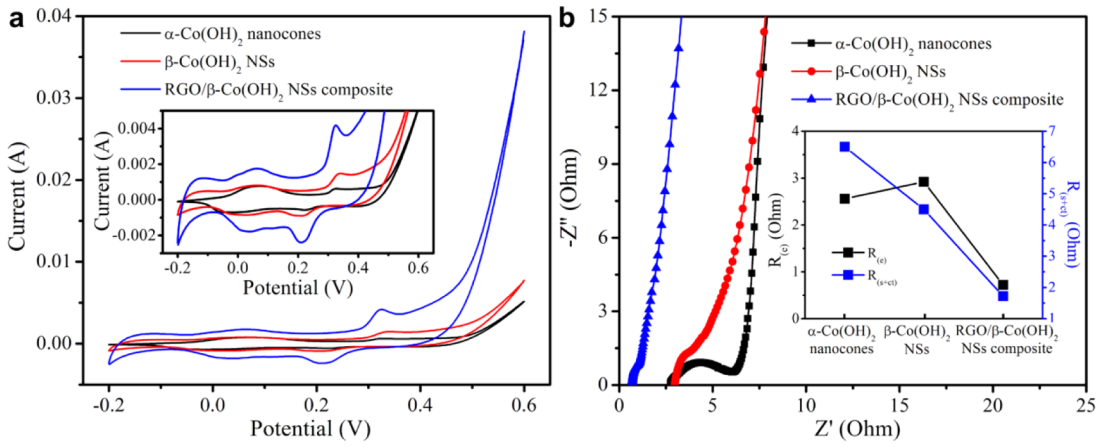

Figure 7. Comparison of electrochemical properties of layered α-Co(OH)$_2$ nanocones, single-layer β-Co(OH)$_2$ NSs, and RGO/β-Co(OH)$_2$ NS composite-based electrode. (a) CV curves at a scan rate of 5 mV/s. (b) Nyquist plots. Inset of panel a shows the blowup of CV curves, and inset of panel b shows the $R_{(e)}$ and $R_{(s+ct)}$ values corresponding to the three electrodes.

than one-electron transfer. As for single-layer β-Co(OH)$_2$ NSs, all active atoms (Co^{2+}) are exposed on surfaces and prone to contact directly with electrolyte. Therefore, both single-layer β-Co(OH)$_2$ NS-based electrodes and RGO/β-Co(OH)$_2$ NS composite-based electrodes exhibit superior electrochemical activity and display an obvious two-electron transferring process. Among them, RGO/β-Co(OH)$_2$ NS composite-based electrodes show the best electrochemical activity with the largest CV area, indicating the biggest capacitance. To investigate the electrode kinetics, the activation energy of the three electrodes was measured from electrochemical impedance spectra (EIS). Figure 7b shows the Nyquist plots of the three electrodes. Their ohmic resistance of the electrolyte and cell components ($R_{(e)}$) are 2.56, 2.92, and 0.72 Ohm for layered α-Co(OH)$_2$ nanocones, single-layer β-Co(OH)$_2$ NSs, and RGO/β-Co(OH)$_2$ NS composite-based electrodes, respectively. The $R_{(e)}$ values of layered α-Co(OH)$_2$ nanocones and single-layer β-Co(OH)$_2$ NS-based electrodes are very closed, but the $R_{(e)}$ of RGO/β-Co(OH)$_2$ NS composite-based electrodes is only 0.72 Ohm. The impedance could be ascribed to the combination of surface and charge-transfer resistance $R_{(s+ct)}$ due to the appearance of a single semicircle. The $R_{(s+ct)}$ values are 6.5, 4.5, and 1.72 Ohm for layered α-Co(OH)$_2$ nanocones, single-layer β-Co(OH)$_2$ NSs, and RGO/β-Co(OH)$_2$ NS composite-based electrodes, respectively. It indicates that the RGO/β-Co(OH)$_2$ NS composite-based electrodes have a faster charge-transfer process than the other two electrodes. Apparently, the introduction of RGO could improve both $R_{(e)}$ and $R_{(s+ct)}$ greatly.

Galvanostatic charge−discharge curves for the three electrodes were tested as shown in Figure 8. The RGO/β-Co(OH)$_2$ NS composite-based electrode gives the largest capacitance of 2080 F/g. The capacitance for layered α-Co(OH)$_2$ nanocones and single-layer β-Co(OH)$_2$ NS-based electrodes is 1055 and 1197 F/g, respectively. It shows that the capacitance of a single-layer

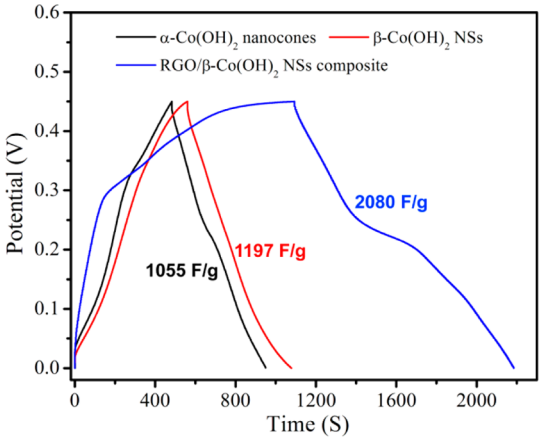

Figure 8. Charge/discharge curves of layered α-Co(OH)$_2$ nanocones, single-layer β-Co(OH)$_2$ NSs, and RGO/β-Co(OH)$_2$ NS composite-based electrodes at the current density of 1 A/g.

β-Co(OH)$_2$ NS-based electrode is only slightly larger than that of layered α-Co(OH)$_2$ nanocone-based electrodes. This is because the single-layer β-Co(OH)$_2$ NSs with high surface energy are prone to restack after drying.[19] The restacking will cause the loss of the electrochemical surface area of single-layer β-Co(OH)$_2$ NSs. The introduction of RGO into β-Co(OH)$_2$ NSs could effectively avoid the stacking of nanosheets and give rise to an excellent electrochemical performance.

Figure 9a shows CV curves of RGO/β-Co(OH)$_2$ NS composite-based electrodes at various scan rates from 5 to 100 mV. Due to the excellent electrochemical activity of RGO/β-Co(OH)$_2$ NS composites, the redox peaks can be clearly observed even at a higher scan rate up to 100 mV. Figure 9b displays the galvanostatic charge−discharge plots of RGO/β-Co(OH)$_2$ NS composites at different current densities. All the curves show symmetric triangular charge−discharge curves with well-defined plateaus, suggesting their good pseudocapacitive behaviors. The specific capacitance of the sample at different current densities was calculated

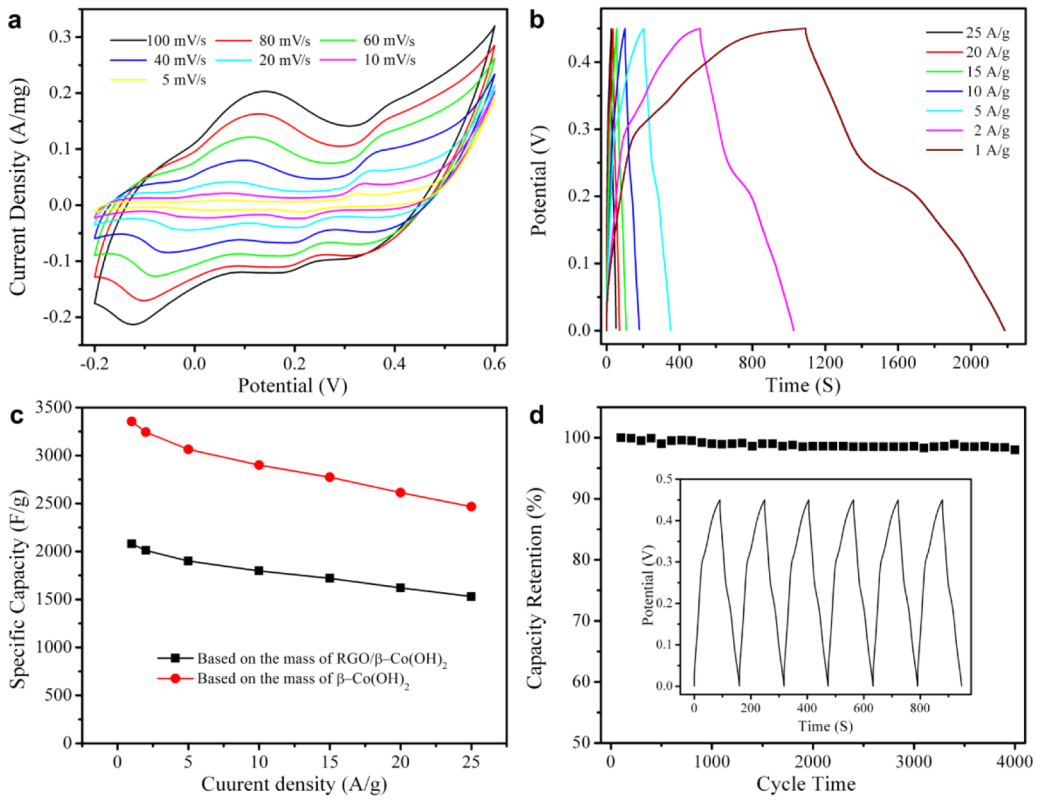

Figure 9. Electrochemical properties of RGO/β-Co(OH)$_2$ NS composite-based electrode. (a) CV curves at different scan rates, (b) charge−discharge curves, (c) specific capacitance at different current densities, and (d) specific capacitance *vs* cycle number of the composite at a current density of 10 A/g (inset of panel d is galvanostatic charge−discharge curves with time).

based on the galvanostatic charge−discharge curves as presented in Figure 9c. The specific capacitances of 2080, 2011, 1900, 1798, 1720, 1620, and 1530 F/g corresponding to the current densities of 1, 2, 5, 10, 15, 20, and 25 A/g are obtained when considering the total mass of the electrode. If scaled to the mass of β-Co(OH)$_2$ NSs, the specific capacitance up to 3355 F/g at the current density of 1 A/g is obtained. Moreover, the RGO/β-Co(OH)$_2$ NS composite-based electrode exhibits an excellent long-life-cycle stability. The galvanostatic charge and discharge curves show that there is no obvious decrease of specific capacitance at a current density of 10 A/g after more than 4000 cycles (Figure 9d). The superior performance of RGO/β-Co(OH)$_2$ NS composite-based electrodes is due to two important aspects. One is the use of single-layer β-Co(OH)$_2$ NSs as active material and another is the function of RGO as an electron conductor. It has been acknowledged that only surface atoms or a very thin layer of active materials play a key role during the pseudocapacitive process. The charge/discharge process can only be localized in a finite volume near the conductive additive. In most of the nanostructured electrodes with a certain volume, electron transport from interior to exterior of active materials is prohibited more or less due to internal resistance, which causes a low utilization of active electrode materials, especially at high charge/discharge rate. Therefore, a quick potential drop across the electrode is often observed. In β-Co(OH)$_2$ NSs, all Co atoms are exposed on the surface and there are no redundant components. The alternative face-to-face assembly of β-Co(OH)$_2$ NSs and RGO gives rise to a maximum contact of Co and RGO basal plane. Once a faradic redox reaction occurs in Co(OH)$_2$, all electrons could be transported onto RGO. As a result, the utilization of faradic redox reaction to capacitance for β-Co(OH)$_2$ NSs could be maximized. The RGO is another key step to improve the electrical conductivity of the whole electrode, thus to achieve high electrode performance. The good conductivity of the electrode is advantageous to depress the loss of specific capacitance at higher current density. For our RGO/β-Co(OH)$_2$ NS composite, a 26.5% loss of the specific capacitance from 2080 to 1530 F/g is obtained when the current density increases from 1 to 25 A/g. This decrease rate is much smaller than previously reported Co(OH)$_2$-based electrodes, indicating the importance of RGO as electron conductor.

DISCUSSION

Since at least Yangshao Culture (Neolithic, 5000−3000 B.C.), where the ancient Chinese used layered clays to make pottery, people have been harnessing the properties of layered materials.[56] This gradually developed into scientific research, leading to the elucidation of the laminar structure of layered materials,

understanding their properties, and eventually fabricating them into individual, atomically/molecularly thin NSs. Recently, due to the inspiration from graphene, 2D materials have attracted great attention and show great potential in many engineering applications, given the excellent in-plane mechanical, structural, thermal, and electrical properties. Nowadays, many layered materials were successfully exfoliated including transition metal oxides, transition metal hydroxides, transition metal dichalcogenides, and other 2D compounds such as BN, Bi_2T_3, Bi_2Se_3, and so on.[57] Apparently, the future prospect for 2D materials is huge, covering a massive range from the most insulating one to the most conductive one and from the strongest one to the softest one. At present, how to use or what should be used for this magic morphology efficiently becomes the major issue.[58−60] Considering that most 2D materials are based on transition metal, it is reasonable to assume that they would be useful in the field of energy conversion and storage due to the good electrochemical activity of transition metals. However, materials for energy conversion or storage, including supercapacitors, lithium ion batteries, and fuel cells, always need to be electrically conductive. Most transition-metal-based 2D materials are electrical insulators or have poor electrical conductivity. In addition, 2D materials are prone to restack owing to their large surface energy. These two aspects block their function in practical application. As demonstrated in this work, the single-layer β-$Co(OH)_2$ NS-based electrode shows similar electrochemical performance to the α-$Co(OH)_2$ nanocone-based electrode due to the restacking of single-layer β-$Co(OH)_2$ NSs. Apparently, an appropriate assembly or integration method is vitally important for the efficient utilization of transition-metal-based 2D materials. Graphene, as a good electrical conductive 2D material with large surface area, is a perfect mate for transition-metal-based 2D materials. Furthermore, assembling the two types of 2D materials by face-to-face form could maximize the contact area for both individuals. This sandwich structure can offer even greater scope by combining the different characteristics of individual layers and tailoring the properties with atomic precision to fit an enormous range of applications. RGO/single-layer cobalt−aluminum hydroxide NS heterostructure has been demonstrated recently by our group as the first model system, which showed very promising electrochemical characteristics.[51] Due to a lack of electrochemical activity of aluminum, single-layer cobalt−aluminum hydroxide NSs are replaced by single-layer cobalt hydroxide NSs in this work. As a result, the RGO/β-$Co(OH)_2$ NS composite exhibits greatly enhanced electrochemical performance. The self-assembly method driven by natural electrostatic force of materials could be easily extended to other 2D materials to design a hybrid structure on demand.

CONCLUSIONS

In summary, we described in this work a new single-layer β-$Co(OH)_2$ NS for the first time and a novel all-2D materials-based pseudocapacitive electrode composed of two kinds of single-layer atom-thick NSs including RGO and β-$Co(OH)_2$. The designed electrode material exhibited superior electrochemical properties, excellent rate performance, and cyclic stability. Our results demonstrated the rationality of our strategy for designing an electrode as a pseudocapacitor and the all-2D materials-based electrodes, which might be one of the most promising candidates for achieving high-performance supercapacitors. Moreover, the two-dimensional characteristic of our electrode gives it an advantage over the other electrodes with porous architectures when considering volume capacity.

METHODS

Preparation of α-$Co(OH)_2$ Nanocones. In a three-necked flask filled with nitrogen gas, $CoCl_2 \cdot 6H_2O$, sodium dodecyl sulfate (SDS), and hexamethylenetetramine (HMT) were dissolved in 1 L of deionized water to give the final concentrations of 5, 20, and 15 mM, respectively. The reaction solution was then heated to 95 °C under magnetic stirring. After 5 h, a green suspension was produced. The product was filtered and washed with deionized water and anhydrous ethanol for several times and finally air-dried at room temperature.

Exfoliation of α-$Co(OH)_2$ Nanocones into Single-Layer β-$Co(OH)_2$ NSs. α-$Co(OH)_2$ nanocones (0.5 g) were mixed with 1 L of formamide and stirred under nitrogen protection at 80 °C for 15 h. To purify exfoliated product, the resulting solution was centrifuged at 8000 rpm for 10 min in order to remove nonexfoliated parts. Our results showed that there is almost no nonexfoliated nanocones remaining in the bottom of the centrifuge tube, and the exfoliation yield is nearly 100%.

Preparation of RGO/β-$Co(OH)_2$ NS Composites. GO was prepared by Hummers' method with little modification (see Supporting Information). Two hundred milliliters of GO water dispersion (0.5 mg/mL) was added to 200 mL of β-$Co(OH)_2$ NS (0.5 mg/mL) formamide dispersion. After that, the precipitate was collected by centrifuging at 6000 rpm for 10 min and washed three times with Milli-Q water. For reduction of GO, the collected product was put in a tube furnace and heated at 180 °C for 1 h under Ar_2/H_2 (5 wt % H_2) mixed gas sphere.

Electrochemical Measurement. Electrochemical measurements were carried out in 2 M aqueous KOH in a half-cell setup configuration at room temperature. Platinum wire and a standard calomel electrode (SCE) served as a counter electrode and a reference electrode, respectively. The working electrode was prepared by casting the slurry containing active materials, carbon black, and polyvinylidene fluoride (PVDF) in a weight ratio of 80:10:10 onto a 1 cm × 1 cm Ni foam (the area for slurry coating is 0.2 cm × 1 cm). The electrodes were dried in vacuum at 80 °C for at least 12 h. The resulting electrode was pressed at 5 MPa for the electrochemical test. The mass of active materials was accurately determined using a microbalance with 0.001 mg resolution (Sartarious). CV curves were recorded with a potential window of −0.2 to 0.6 V *vs* SCE. EIS was collected by applying a perturbation voltage of 5 mV in a frequency range of 100 kHz to 10 mHz.

Conflict of Interest: The authors declare no competing financial interest.

Acknowledgment. This work was supported by the National Natural Science Foundation of China (Grant No. 21273270), the National Basic Research Program of China (2013CB933000), the Key Development Project of Chinese Academy of Sciences (No. KJZD-EW-M01-3), and the Natural Science Foundation of Jiangsu Province (BK20130007).

Supporting Information Available: Preparation and characterization of GO, zeta-potential of GO, $Co(OH)_2$ NSs, TG of RGO/β-$Co(OH)_2$ NS composites. This material is available free of charge *via* the Internet at http://pubs.acs.org.

REFERENCES AND NOTES

1. Novoselov, K. S.; Geim, A. K.; Morozoc, S. V.; Jiang, D.; Zhang, Y.; Dubonos, S. V.; Grigorieva, I. V.; Firsov, A. A. Electric Field Effect in Atomically Thin Carbon Films. *Science* **2004**, *22*, 666–669.
2. Novoselov, K. S.; Geim, A. K.; Morozov, S. V.; Jiang, D.; Katsnelson, M. I.; Grigorieva, I. V.; Dubonos, S. V.; Firsov, A. A. Two-Dimensional Gas of Massless Dirac Fermions in Graphene. *Nature* **2005**, *438*, 197–200.
3. Geim, A. K.; Novoselov, K. S. The Rise of Graphene. *Nat. Mater.* **2007**, *6*, 183–191.
4. Novoselov, K. S.; Jiang, Z.; Zhang, Y.; Morozov, S. V.; Stormer, H. L.; Zeitler, U.; Maan, J. C.; Boebinger, G. S.; Kim, P.; Geim, A. K. Room-Temperature Quantum Hall Effect in Graphene. *Science* **2007**, *9*, 1379.
5. Service, R. F. Carbon Sheets an Atom Thick Give Rise to Graphene Dreams. *Science* **2009**, *15*, 875–877.
6. Li, X.; Wang, X.; Zhang, L.; Lee, S.; Dai, H. Chemically Derived, Ultrasmooth Graphene Nanoribbon Semiconductors. *Science* **2008**, *319*, 1229–1232.
7. Hernander, Y.; Nicolosi, V.; Lotya, M.; Blighe, F. M.; Sun, Z.; De, S.; Mcgovern, I. T.; Holland, B.; Byrne, M.; Gun'Ko, Y. K.; *et al.* High-Yield Production of Graphene by Liquid-Phase Exfoliation of Graphite. *Nat. Nanotechnol.* **2008**, *3*, 563–568.
8. Li, X.; Cai, W.; An, J.; Kim, S.; Nah, J.; Yang, D.; Piner, R.; Velamakanni, A.; Jung, I.; Tutuc, E.; *et al.* Large-Area Synthesis of High-Quality and Uniform Graphene Films on Copper Foil. *Science* **2009**, *324*, 1312–1314.
9. Chen, Z. P.; Ren, W. C.; Gao, L. B.; Liu, B. L.; Pei, S. F.; Cheng, H. M. Three-Dimensional Flexible and Conductive Interconnected Graphene Networks Grown by Chemical Vapor Deposition. *Nat. Mater.* **2011**, *10*, 424–428.
10. Mak, K. F.; Lee, C.; Hone, J.; Shan, J.; Heinz, T. F. Atomically Thin MoS_2: A New Direct-Gap Semiconductor. *Phys. Rev. Lett.* **2010**, *105*, 136805.
11. Du, D. X.; Hor, Y. S.; Xiong, J.; Cava, R. J.; Ong, N. P. Quantum Oscillations and Hall Anomaly of Surface States in the Topological Insulator Bi_2Te_3. *Science* **2010**, *329*, 821–824.
12. Kong, D.; Chen, Y.; Cha, J. J.; Zhang, Q.; Analitis, J. G.; Lai, K.; Liu, Z.; Hong, S. S.; Koski, K. J.; Mo, S.-K.; *et al.* Ambipolar Field Effect in the Ternary Topological Insulator $(Bi_xSb_{1-x})Te_3$ by Composition Tuning. *Nat. Nanotechnol.* **2011**, *6*, 705–709.
13. Wang, Q. H.; Kalantar-Zadeh, K.; Kis, A.; Coleman, J. N.; Strano, M. S. Electronics and Photo-electronics of Two-Dimensional Transition Metal Dichalcogenides. *Nat. Nanotechnol.* **2012**, *7*, 699–712.
14. Zeng, H.; Dai, J.; Yao, W.; Xiao, D.; Cui, X. Valley Polarization in MoS_2 Monolayers by Optical Pumping. *Nat. Nanotechnol.* **2012**, *7*, 490–493.
15. Kim, J.; Byun, S.; Smith, A. J.; Yu, J.; Huang, J. Enhanced Electrocatalytic Properties of Transition-Metal Dichalcogenides Sheets by Spontaneous Gold Nanoparticle Decoration. *J. Phys. Chem. Lett.* **2013**, *4*, 1227–1232.
16. Bianco, E.; Butler, S.; Jiang, S.; Restrepo, O. D.; Windl, W.; Goldberger, J. E. Stability and Exfoliation of Germanane: A Germanium Graphene Analogue. *ACS Nano* **2013**, *7*, 4414–4421.
17. Koski, K. J.; Cui, Y. The New Skinny in Two-Dimensional Nanomaterials. *ACS Nano* **2013**, *7*, 3739–3743.
18. Omomo, Y.; Sasaki, T.; Wang, L.; Watanabe, M. Redoxable Nanosheet Crystallites of MnO_2 Derived *via* Delamination of a Layered Manganese Oxide. *J. Am. Chem. Soc.* **2003**, *125*, 3568–3575.
19. Liu, Z.; Ma, R.; Osada, M.; Iyi, N.; Ebina, Y.; Takada, K.; Sasaki, T. Synthesis, Anion Exchange, and Delamination of Co–Al Layered Double Hydroxide: Assembly of the Exfoliated Nanosheet/Polyanion Composite Films and Magneto-optical Studies. *J. Am. Chem. Soc.* **2006**, *128*, 4872–4880.
20. Ma, R.; Liu, Z.; Takada, K.; Iyi, N.; Bando, Y.; Sasaki, T. Synthesis and Exfoliation of Co^{2+}–Fe^{3+} Layered Double Hydroxides: An Innovative Topochemical Approach. *J. Am. Chem. Soc.* **2007**, *129*, 5257–5263.
21. Ma, R.; Sasaki, T. Nanosheets of Oxides and Hydroxides: Ultimate 2D Charge-Bearing Functional Crystallites. *Adv. Mater.* **2010**, *22*, 5082–5104.
22. Ma, R.; Liang, J.; Takara, K.; Sasaki, T. Topochemical Synthesis of Co–Fe Layered Double Hydroxides at Varied Fe/Co Ratios: Unique Intercalation of Triiodide and Its Profound Effect. *J. Am. Chem. Soc.* **2011**, *133*, 613–620.
23. Ma, R.; Liang, J.; Liu, X.; Sasaki, T. General Insights into Structural Evolution of Layered Double Hydroxide: Underlying Aspects in Topochemical Transformation from Brucite to Layered Double Hydroxide. *J. Am. Chem. Soc.* **2012**, *134*, 19915–19921.
24. Wang, Q.; O'Hare, D. Recent Advances in the Synthesis and Application of Layered Double Hydroxide (LDH) Nanosheets. *Chem. Rev.* **2012**, *112*, 4214–4155.
25. Osada, M.; Sasaki, T. Two-Dimensional Dielectric Nanosheets: Novel Nanoelectronics from Nanocrystal Building Blocks. *Adv. Mater.* **2012**, *24*, 210–228.
26. Geng, F.; Matsushita, Y.; Ma, R.; Xin, H.; Tanaka, M.; Izumi, F.; Iyi, N.; Sasaki, T. General Synthesis and Structural Evolution of a Layered Family of $Ln_8(OH)_2Cl_4 \cdot nH_2O$ (Ln = Dd, Sm, Eu, Gd, Tb, Dy, Ho, Er, Tm, and Y). *J. Am. Chem. Soc.* **2008**, *130*, 16344–16350.
27. Lee, C.; Li, Q.; Kalb, W.; Liu, X. Z.; Berger, H.; Carpick, R. W.; Hone, J. Frictional Characteristics of Atomically Thin Sheets. *Science* **2010**, *328*, 76–80.
28. Geng, F.; Ma, R.; Sasaki, T. Anion-Exchange Layered Materials Based on Rare-Earth Phosphor: Unique Combination of Rare-Earth Host and Exchangeable Anions. *Acc. Chem. Res.* **2010**, *43*, 1177–1185.
29. Coleman, J. N.; Lotya, M.; O'Neill, A.; Bergin, S. D.; King, P. J.; Khan, U.; Young, K.; Gaucher, A.; De, S.; Smith, R. J.; *et al.* Two-Dimensional Nanosheets Produced by Liquid Exfoliation of Layered Materials. *Science* **2011**, *331*, 568–571.
30. Kong, D.; Cui, Y. Opportunities in Chemistry and Materials Science for Topological Insulators and Their Nanostructures. *Nat. Chem.* **2011**, *3*, 845–849.
31. Zeng, Z.; Yin, Z.; Huang, X.; Li, H.; He, Q.; Lu, G.; Boey, F.; Zhang, H. Single-Layer Semiconducting Nanosheets: High-Yield Preparation and Device Fabrication. *Angew. Chem., Int. Ed.* **2011**, *50*, 11093–11097.
32. Huang, X.; Li, H.; Li, S.; Wu, S.; Boey, F.; Zhang, H. Synthesis of Gold Square-like Plates from Ultrathin Gold Square Sheets: The Evolution of Structure Phase and Shape. *Angew. Chem., Int. Ed.* **2011**, *50*, 12245–12248.
33. Huang, X.; Tang, S.; Mu, X.; Dai, Y.; Chen, G.; Zhou, Z.; Ruan, F.; Yang, Z.; Zheng, N. Freestanding Palladium Nanosheets with Plasmonic and Catalytic Properties. *Nat. Nanotechnol.* **2011**, *6*, 28–32.
34. Zhang, X. D.; Zhang, J.; Zhao, J.; Pan, B.; Kong, M.; Chen, J.; Xie, Y. Half-Metallic Ferromagnetism in Synthetic Co_9Se_8 Nanosheets with Atomic Thickness. *J. Am. Chem. Soc.* **2012**, *134*, 11908–11911.
35. Zhang, X.; Xie, X.; Wang, H.; Zhang, J.; Pan, B.; Xie, Y. Enhanced Photoresponsive Ultrathin Graphitic-Phase C_3N_4 Nanosheets for Bioimaging. *J. Am. Chem. Soc.* **2013**, *135*, 18–21.
36. Rui, X.; Zhao, X.; Lu, Z.; Tan, H.; Sim, D.; Hng, H. H.; Yazami, R.; Lim, T. M.; Yan, Q. Olivine-Type Nanosheets for Lithium Ion Battery Cathodes. *ACS Nano* **2013**, *7*, 5637–5646.

37. Jiang, H.; Tan, K. J.; Zhang, K. K.; Chen, X.; Kloc, C. Ultrathin Organic Single Crystals: Fabrication, Field-Effect Transistor and Thickness Dependence of Charge Carrier Mobility. *J. Mater. Chem.* **2011**, *21*, 4771–4773.
38. Bish, D. L.; Livingstore, A. The Crystal Chemistry and Paragenesis of Honessite and Hydrohonessite: The Sulphate Analogues of Reevesite. *Miner. Mag.* **1981**, *44*, 339–343.
39. Liu, X.; Ma, R.; Bando, Y.; Sasaki, T. Layered Cobalt Hydroxide Nanocones: Microwave-Assisted Synthesis, Exfoliation, and Structural Modification. *Angew. Chem., Int. Ed.* **2010**, *49*, 8253–8256.
40. Liu, Z.; Ma, R.; Osada, M.; Takada, K.; Sasaki, T. Selective and Controlled Synthesis of α- and β-Cobalt Hydroxides in Highly Developed Hexagonal Platelets. *J. Am. Chem. Soc.* **2005**, *127*, 13869–13874.
41. Ma, R.; Takada, K.; Fukuda, K.; Iyi, N.; Bando, Y.; Sasaki, T. Topochemical Synthesis of Monometallic (Co^{2+}—Co^{3+}) Layered Double Hydroxide and Its Exfoliation into Positively Charged $Co(OH)_2$ Nanosheets. *Angew. Chem., Int. Ed.* **2008**, *47*, 86–89.
42. Chen, S.; Zhu, J. W.; Wang, X. One-Step Synthesis of Graphene-Cobalt Hydroxide Nanocomposites and Their Electrochemical Properties. *J. Phys. Chem. C* **2010**, *114*, 11829–11834.
43. Zhao, M. Q.; Zhang, Q.; Huang, J. Q.; Wei, F. Hierarchical Nanocomposites Derived from Nanocarbons and Layered Double Hydroxides—Properties, Synthesis, and Applications. *Adv. Funct. Mater.* **2012**, *22*, 675–694.
44. Dong, X.; Wang, L.; Wang, D.; Li, C.; Jin, J. Layer-by-Layer Engineered Co−Al Hydroxide Nanosheets/Graphene Multilayer Films as Flexible Electrode for Supercapacitor. *Langmuir* **2012**, *28*, 293–298.
45. Cao, L.; Xu, F.; Liang, Y. Y.; Li, H. L. Preparation of the Novel Nanocomposite $Co(OH)_2$/Ultra-stable Y Zeolite and Its Application as a Supercapacitor with High Energy Density. *Adv. Mater.* **2004**, *16*, 1853–1857.
46. Yuan, C.; Zhang, X.; Hou, L.; Shen, L.; Li, D.; Zhang, F.; Fan, C.; Li, J. Lysine-Assisted Hydrothermal Synthesis of Urchin-like Ordered Arrays of Mesoporous $Co(OH)_2$ Nanowires and Their Application in Electrochemical Capacitors. *J. Mater. Chem.* **2010**, *20*, 10809–10816.
47. Xia, X. H.; Tu, J. P.; Zhang, Y. Q.; Mai, Y. J.; Wang, X. L.; Gu, C. D.; Zhao, X. B. Three-Dimentional Porous Nano-Ni/$Co(OH)_2$ Nanoflake Composite Film: A Pseudocapacitive Material with Superior Performance. *J. Phys. Chem. C* **2011**, *115*, 22662–22668.
48. Zhao, C.; Wang, X.; Wang, S.; Wang, Y.; Zhao, Y.; Zheng, W. Synthesis of $Co(OH)_2$/Graphene/Ni Foam Nano-electrodes with Excellent Pseudocapacitive Behavior and High Cycling Stability for Supercapacitors. *Int. J. Hydrogen Energy* **2012**, *37*, 11846–11852.
49. Zhao, C.; Zheng, W.; Wang, X.; Zhang, H.; Cui, X.; Wang, H. Ultrahigh Capacitive Performance from Both $Co(OH)_2$/Graphene Electrode and $K_3Fe(CN)_6$ Electrolyte. *Sci. Rep.* **2013**, *3*, 2986.
50. Wang, L.; Dong, Z. H.; Wang, Z. G.; Zhang, F. X.; Jin, J. Layered α-$Co(OH)_2$ Nanocones as Electrode Materials for Pseudocapacitors: Understanding the Effect of Interlayer Space on Electrochemical Activity. *Adv. Funct. Mater.* **2013**, *23*, 2758–2764.
51. Wang, L.; Wang, D.; Dong, X.; Zhang, Z.; Pei, X.; Chen, X.; Chen, B.; Jin, J. Layered Assembly of Graphene Oxide and Co−Al Layered Double Hydroxide Nanosheets as Electrode Materials for Supercapacitors. *Chem. Commun.* **2011**, *47*, 3556–3558.
52. Niu, Z.; Du, J.; Cao, X.; Sun, Y.; Zhou, W.; Hng, H. H.; Ma, J.; Chen, X.; Xie, S. Electrophoretic Build-up of Alternately Multilayered Films and Micropatterns Based on Graphene Sheets and Nanoparticles and Their Applications in Flexible Supercapacitors. *Small* **2012**, *8*, 3201–3208.
53. Niu, Z.; Chen, J.; Hng, H. H.; Ma, J.; Chen, X. A Leavening Strategy To Prepare Reduced Graphene Oxide Foams. *Adv. Mater.* **2012**, *24*, 4144–4150.
54. Niu, Z.; Zhang, L.; Liu, L.; Zhu, B.; Dong, H.; Chen, X. All-Solid-State Flexible Ultrathin Micro-supercapacitors Based on Graphene. *Adv. Mater.* **2013**, *25*, 4035–4042.
55. Schmelzer, J.; Moller, J.; Gutzow, I. Ostwald's Rule of Stages: The Effect of Elastic Strains and External Pressure. *Z. Phys. Chem.* **1998**, *204*, 171–181.
56. Lawler, A. *Science* **2009**, *325*, 930–935.
57. Nicolosi, V.; Chhowalla, M.; Kanatzidis, M. G.; Strano, M. S.; Coleman, J. N. Liquid Exfoliation of Layered Materials. *Science* **2013**, *340*, 1420.
58. Yang, M.; Hou, Y.; Kotov, N. A. Graphene-Based Multilayers: Critical Evaluation of Materials Assembly Techniques. *Nano Today* **2012**, *7*, 430–447.
59. Novoselov, K. S.; Fal'ko, V. I.; Colombo, L.; Gellert, P. R.; Schwab, M. G.; Kim, K. A Roadmap of Graphene. *Nature* **2013**, *490*, 192–200.
60. Tang, Z.; Kotov, N. A.; Magonov, S.; Ozturk, B. Nanostructured Artificial Nacre. *Nat. Mater.* **2003**, *2*, 413–418.